



# Structural and optical properties of copper oxide nanoparticles: A study of variation in structure and antibiotic activity

Ankush Chauhan<sup>1</sup>, Ritesh Verma<sup>1</sup>, Khalid Mujasam Batoo<sup>2,a)</sup> , Swati Kumari<sup>3</sup>, Rahul Kalia<sup>1</sup>, Rajesh Kumar<sup>1,4,a)</sup>, Muhammad Hadi<sup>5</sup>, Emad H. Raslan<sup>5</sup>, Ahamad Imran<sup>3</sup>

<sup>1</sup>School of Physics and Materials Science, Shoolini University of Biotechnology & Management Sciences, Bajhol-Solan, HP 173212, India

<sup>2</sup>King Abdullah Institute for Nanotechnology, King Saud University, P.O. Box 2455, Riyadh 11451, Saudi Arabia

<sup>3</sup>School of Applied Science and Biotechnology, Shoolini University of Biotechnology & Management Sciences, Bajhol-Solan, HP 173212, India

<sup>4</sup>Himalayan Centre of Excellence for Nanotechnology, Shoolini University of Biotechnology & Management Sciences, Bajhol-Solan, HP 173212, India

<sup>5</sup>Department of Physics and Astronomy, King Saud University, P.O. Box 2455, Riyadh 11451, Saudi Arabia

<sup>a)</sup>Address all correspondence to these authors. e-mails: khalid.mujasam@gmail.com kbatoo@ksu.edu.sa; rajeshsharma@shooliniuniversity.com

Received: 13 February 2021; accepted: 28 March 2021; Published online: 19 April 2021

In this paper, we study the synthesis dependence of structural, optical and antimicrobial properties for copper oxide nanoparticles on, synthesized using microwave irradiation CuO(M), co-precipitation CuO(P) and hydrothermal CuO(H) protocols. Structural and morphological properties were studied using XRD, SEM, TEM and SAED techniques. XPS studies confirmed the presence of copper ions in Cu<sup>2+</sup> oxidation state, and Raman spectroscopy confirmed the presence of nanostructured phase in all the samples. The synthesized CuO(M), CuO(P) and CuO(H) nanoparticles were investigated for antimicrobial activity against different pathogenic bacteria including methicillin-resistant *Staphylococcus aureus*. The result showed that maximum inhibition zone was detected in CuO(M) nanoparticles against Gram-negative bacteria i.e. *Klebsiella pneumoniae* (20 mm). CuO(H) and CuO(P) nanoparticles have antibacterial inhibition zone of 17 mm and 13 mm against *K. pneumoniae* and *S. aureus*, respectively. The CuO(P) and CuO(H) nanoparticles displayed mild antimicrobial activity as compared to the CuO(M) nanoparticles.

## Introduction

In recent years, intrigue has developed in the field of research in metal oxide nanoparticles due to its vast scope of utilization in catalysis, optoelectronics, biotechnology, nanodevices, nanoelectronics, wastewater treatment, nanosensors and data stockpiling [1–6]. The bewildering applications of nanomaterials have encouraged their utilization in the expulsion of different perilous contaminants from water, for example, substantial metals, antimicrobial specialists, colours and other natural contaminants [7–10]. Interestingly, varieties of metal oxides are accessible, but some of them are widely studied by researchers owing to the numerous applications that cannot be satiated by the natural abundance and compel an innovative approach to obtain it.

Moreover, it is well reported in the literature that the synthetic protocol applied for the preparation of nanoparticles plays an important role in the shape and size of the nanoparticles obtained. For example, Toma et al. carried out a detailed study

towards the effect of the synthetic procedure on the catalytic performance on Au nanoparticles. It was found by Kimling et al. that varying the molar ratio between trisodium citrate and chloroauric acid impacted the size of the nanoparticles formed [11]. Similarly, it was also found that surfactant-based synthesis also affects the morphology of nanoparticles obtained [12]. In an interesting study reported by Li et al., it was found that hydrothermal and solvothermal yielded nanoparticles with different thermoelectric properties [13]. Moreover, it was confirmed by Cheon and coworkers that the shape of the nanoparticles plays an important role in the efficiency/efficacy as an antimicrobial agent [14].

Furthermore, among the various metal oxides reported in the literature, CuO, a transition metal oxide with monoclinic structure and narrow band gap of 1.2 eV has gained attention due to its various applications such as energy harvesting applications [15, 16], colour-sharpened solar cells [17], Li-particle

battery [18], gas detecting [19], antimicrobial action [20, 21] CO<sub>2</sub> adsorption [22], colour expulsion [23] and anticancer studies [24, 25]. Interestingly, CuO nanoparticles owing to the wide range of applications have been synthesized by utilizing diversified methodologies such as sol-gel, quick precipitation, sonochemical, electrochemical, solid-state reaction and microwave irradiation; however, no comparative investigation was carried out in finding out the effect of these synthetic methodologies on the morphology and properties of the obtained CuO nanoparticles [2, 26–30].

Hence, in this work presented, we have studied the effect of synthetic protocols employed for the CuO nanoparticles on the structural composition and antimicrobial properties. In this study, CuO nanoparticles were prepared using three synthetic techniques, i.e. microwave irradiation CuO(M), co-precipitation CuO(P) and hydrothermal method CuO(H), which are characterized using FTIR, XRD, XPS, SEM, EDX and TEM to understand the effect of the synthetic methodology on the structural and morphological properties. Further, the CuO nanoparticles synthesized using various methods were tested for comparative

antimicrobial activities, against Gram positive, i.e. *Staphylococcus aureus* and also against its drug-resistant strain, i.e. methicillin-resistant *Staphylococcus aureus* and Gram-negative bacterial strains, i.e. *Pseudomonas aeruginosa*, *Klebsiella pneumoniae* and *Salmonella typhi*, and the results obtained are discussed in this paper.

## Results and discussion

### X-ray diffraction

X-ray diffraction for the as prepared shows that all the samples exhibit characteristic peaks of the monoclinic structure corresponding to reflection planes (110), (−111), (111), (−202), (020), (202), (−113) and (022) which are in good agreement with JCPDS file no. 05-0661 as shown in Fig. 1a. The CuO(M) peaks were found much broader, which show lower crystallite size of the nanoparticles in comparison to other samples and high crystalline order.

The particle size was calculated using the Scherrer formula [31] and are presented in Table 1.

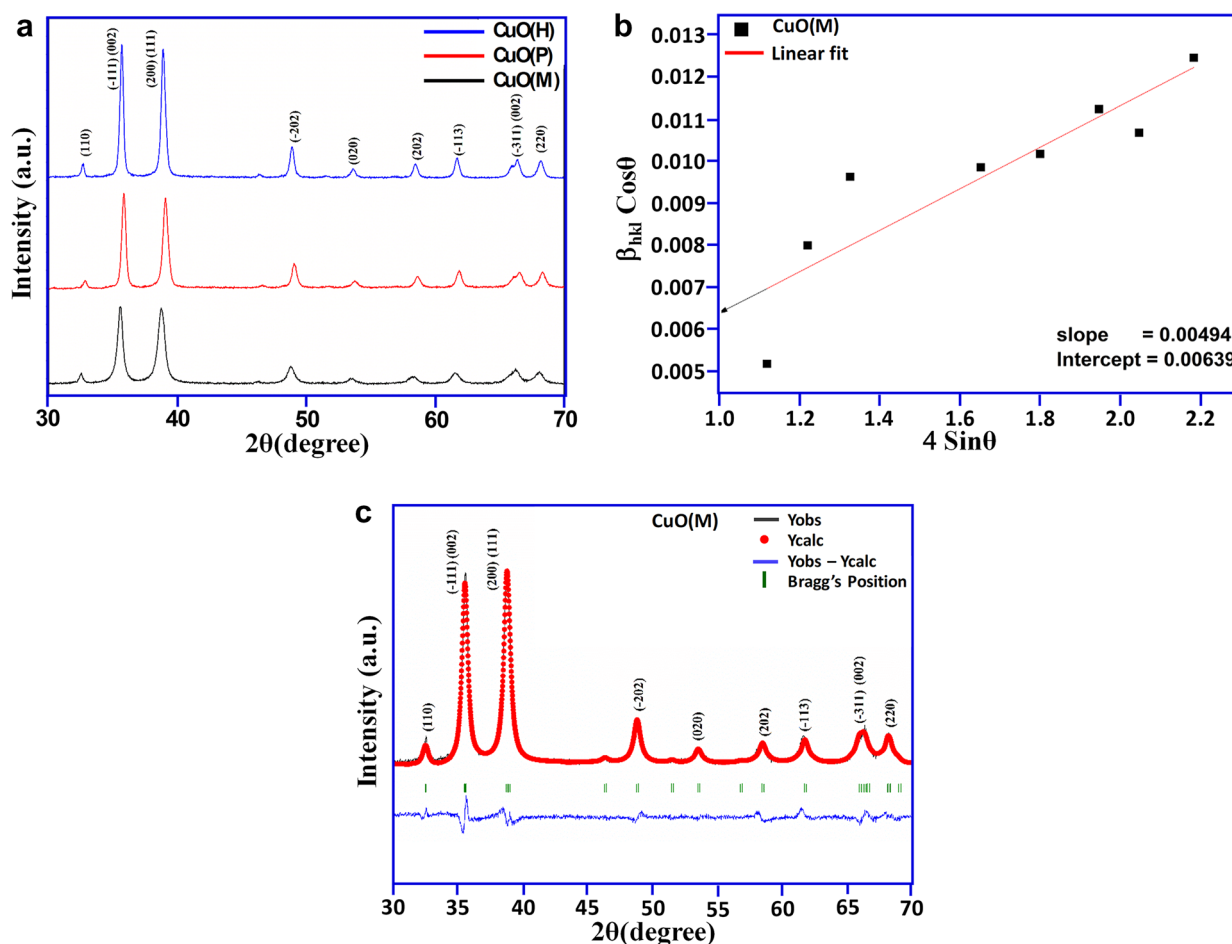


**Figure 1:** (a) XRD pattern of CuO nanoparticles, (b) William-Hall (UDM) plot for CuO (M) nanoparticles and (c) Rietveld refinement of XRD patterns for the CuO(M) nanoparticles.

**TABLE 1:** Structural parameters calculated from the Rietveld refinement.

(CuO)	CuO(M)	CuO(P)	CuO(H)
Structure	Monoclinic	Monoclinic	Monoclinic
Space group	C12/c1	C12/c1	C12/c1
Lattice parameters			
<i>a</i> (Å)	4.686	4.688	4.687
<i>b</i> (Å)	3.424	3.341	3.426
<i>c</i> (Å)	5.118	5.131	5.130
Volume (Å) <sup>3</sup>	80.992	81.383	81.262
Atomic coordinates			
Cu			
<i>x</i>	0.2500	0.2500	0.2500
<i>y</i>	0.2500	0.2500	0.2500
<i>z</i>	0.0000	0.0000	0.0000
O			
<i>x</i>	0.0000	0.0000	0.0000
<i>y</i>	0.4280	0.4195	0.4171
<i>z</i>	0.2500	0.2500	0.2500
Refined parameters			
$\chi^2$	2.469	1.702	1.790
<i>R</i> <sub>p</sub>	17.1	16.2	13.9
<i>R</i> <sub>wp</sub>	15.4	13.1	11.9
<i>R</i> <sub>e</sub>	9.79	10	8.89
Average crystallite size (Scherrer method) (nm)	15.98 ± 2	23.02 ± 3.2	21.88 ± 1
Crystallite size (W-H method) (nm)	21.12	35.15	30.96
Strain ( $\mathcal{E}$ )	0.00494	0.00434	0.0035
Dislocation density	0.0039	0.0018	0.0020

$$D = \frac{0.9\lambda}{\beta \cos\theta}, \quad (1)$$

where *D* is the average crystallite size,  $\lambda$  is the X-ray wavelength,  $\theta$  is the Bragg angle and  $\beta$  is full width at half-maximum FWHM. The crystallite size of CuO nanoparticles synthesized using variable techniques was significantly different. The broader XRD peaks reveal comparatively lower crystallite size of CuO(M) nanoparticles, while the intense sharp peaks of CuO(H) and CuO(P) show the presence of larger crystallite size and higher crystallinity.

The structural parameters ascertained from the XRD pattern obtained are given in Table 1; moreover, the dislocation density *S* listed therein was calculated using Eq. (2) and gives the measure of defects in crystalline structures [32].

$$S = \frac{1}{D^2}. \quad (2)$$

The lattice strain and crystallite size were determined by employing the Universal Deformation Model with the help of William-Hall equation given below [33, 34]:

$$\beta \cos\theta = \frac{k\lambda}{D} + 4\mathcal{E} \sin\theta, \quad (3)$$

where  $\beta$  is (FWHM), *D* is the crystallite size and  $\mathcal{E}$  is the strain. The UDM model considers the isotropic nature of the crystal where the strain is assumed uniform in all crystallographic directions and independent of the direction in which material property is measured. The lattice strain was calculated from the slope, and the intercept gives the crystallite size by plotting  $\beta \cos\theta$  against  $4\mathcal{E} \sin\theta$  using linear fitting as shown in Fig. 1b. The plots obtained for the CuO(P) and CuO(H) are given in the supplementary section Fig. S1.

The crystallite sizes obtained from Scherrer method are comparably smaller than obtained from William-hall method that is because the *W-H* method considers microstrain while as in Scherrer method, we measure the cohesion length of the X-rays, and samples with any defects and vacancies will have smaller crystallite size than the actual [35, 36]. Figure S2 shows the effect of synthesis techniques on the CuO nanoparticles on crystallite size and strain.

Rietveld refinement of all the XRD patterns was performed using Fullprof program with space group C12/c1. The peak patterns were described by pseudo-Voigt profiles, and the background was fitted with linear interpolation. First, global parameters such as background, instrumental and scale factors were refined and then cell parameters. Sequential refinement of FWHM parameters, shape parameters, preferred orientation

and atomic positions were carried out. There is an ascending pattern observed in the lattice parameters and crystallinity in the order CuO(M) < CuO(H) < CuO(P) which suggests that the synthetic protocols adopted and conditions such as the temperature and pressure greatly affected the lattice parameters of the CuO nanoparticles obtained. In the case of CuO(P) nanoparticles, larger particle size is obtained due to calcination temperature, which allowed the densification and grain growth of nanoparticles as confirmed from TEM; however, in the case of CuO(M) nanoparticles small crystallite size obtained can be attributed to in situ synthesis of CuO nanoparticles, where particles are crystallized without diffusion due to the action of microwave radiation [37]. CuO(H) nanoparticles were synthesized in the hydrothermal autoclave which also takes into account the pressure along with heat for the uniform synthesis of nanoparticle, and it has been confirmed from SEM and XRD analysis. Figure 1c shows the Rietveld analysis of CuO(M) and the Rietveld analysis of CuO(P) and CuO(H) is given in the supplementary section Fig. S3.

### XPS analysis

The Cu2p and O1s XPS spectra of CuO(M) nanoparticles are shown in Fig. 2a and b, while the O1s XPS spectra of CuO(P) and CuO(H) nanoparticles are given in supplementary data Fig. S4. The Cu2p spectra reveal Cu2p<sub>3/2</sub> peaks at 933.6 ± 0.2 eV and Cu2p<sub>1/2</sub> at 953.5 ± 0.3 eV for the prepared samples as mentioned in Table 2 and confirm the presence of Cu<sup>2+</sup> species along with the presence of shakeup satellite peaks at ~ 962 eV and ~ 942 eV, respectively, confirming the characteristic presence of Cu<sup>2+</sup> species. The O1s spectra of three CuO nanoparticles as prepared samples show an asymmetric curve which reveals three components after Gaussian fitting, i.e. O<sub>L</sub>, O<sub>V</sub> and O<sub>C</sub> corresponding to the lattice oxygen, oxygen vacancy and chemisorbed or dissociated oxygen species (O<sup>-</sup>, O<sub>2</sub><sup>-</sup> or O<sup>2-</sup>), respectively [38]. It can

**TABLE 2:** Binding energy of core shell level 2p and 10s spectra.

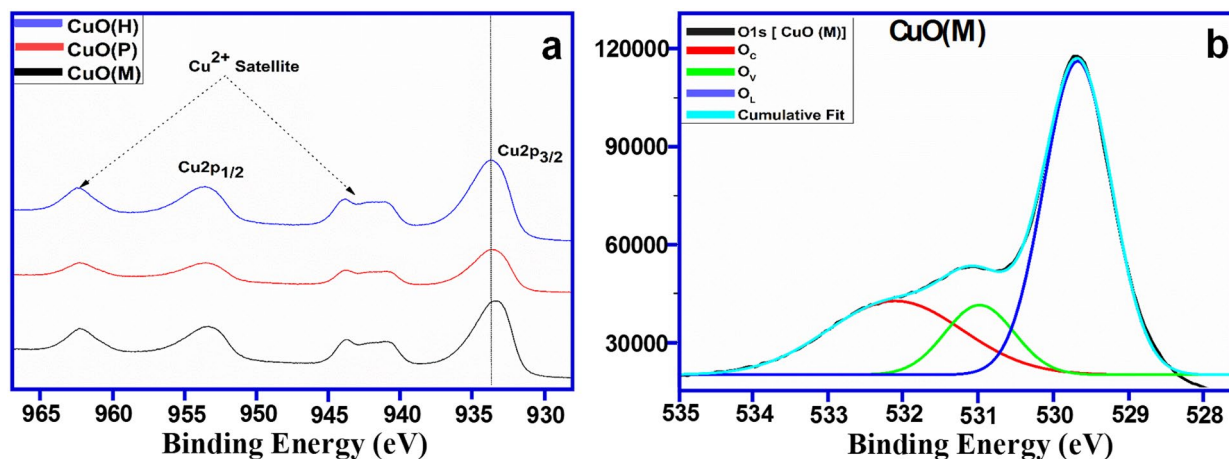
Core shell level	Binding energy (eV) [Percentage]		
	CuO (M)	CuO (P)	CuO (H)
Cu 2P <sub>3/2</sub>	933.35	933.52	933.61
O1s			
O <sub>L</sub>	529.6 [59%]	529.7 [64.3%]	529.7 [60.78%]
O <sub>V</sub>	530.9 [14%]	531.6 [35.7%]	531.1 [22.52%]
O <sub>C</sub>	532.1 [27%]		532.3 [16.70%]

be seen that CuO nanoparticles prepared using co-precipitation method, i.e. CuO(P), do not yield the O<sub>C</sub> component, while it is available in rest of the samples, which can be due to the calcination of the sample, while the highest amount of oxygen vacancies is found in the same sample, i.e. CuO(P) as shown in Table 2.

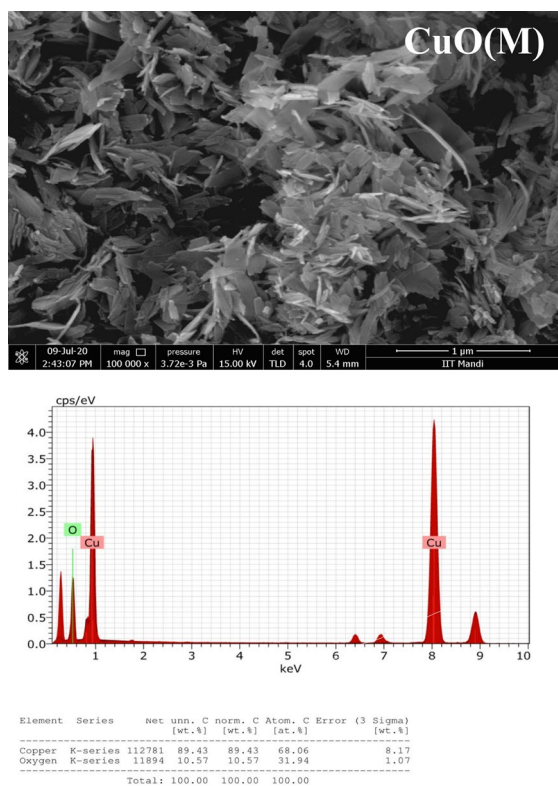
### SEM analysis

Figure 3 shows morphological studies and elemental analysis (EDAX) of as-grown CuO (M) nanoparticles. The SEM image of CuO(M) nanoparticles exhibits feather-like morphology with agglomeration. The CuO(H) nanoparticles appear to possess a 2D-sheet like structures stacked together, whereas the CuO(P) nanoparticles appear to have an irregular diffused nanoplates like morphology, as shown in Figs. S5 and S6.

The EDAX spectrum of CuO(P) and CuO(H) nanoparticles are given in Figure S5 and S6 as supplementary data. The EDAX analysis of the CuO(M), CuO(P) and CuO(H) reveals the presence of elements copper and oxygen. However, the percentage of oxygen in the oxide was found to vary in the samples prepared by varying the synthetic protocol. The least percentage of bonded oxygen was observed in the case of CuO(P) nanoparticles, when compared to other two CuO nanoparticles, i.e. CuO(H) and CuO(M) as confirmed by the XPS analysis.



**Figure 2:** (a) Cu2p XPS spectra and (b) O1s spectra of CuO(M) nanoparticles.



**Figure 3:** SEM and EDAX image of CuO(M) nanoparticles.

The reason for lower oxygen vacancy can be attributed to the calcination of the sample at 400 °C, as per the synthetic protocol followed for the preparation of the nanoparticles.

### TEM analysis

The prepared samples were subjected to TEM analysis to ascertain the variation of shape and size nanoparticles due to the different synthetic protocols employed and the images obtained are given in Fig. 4a–c. From the analysis of the CuO(M), i.e. CuO nanoparticles prepared to employ microwave methodology, the agglomerated grains with an average grain size of 38 nm are formed. However, the other two protocols employed with the other two methodologies, it was found that the CuO(H) nanoparticles formed were found to be a uniform grain of 420 nm dimension with distinguishable grain boundaries; moreover, the CuO(P) nanoparticles were found to possess smaller grains diffused to form larger grains during calcination process with an average grain size of 234 nm, which were mostly agglomerated grains.

The SAED pattern of nanoparticles was obtained, and it was found that the CuO(M) nanoparticles form continuous rings with bright spots confirming poly and nanocrystalline nature of the nanoparticles. On the other hand, widened diffraction rings with scattered diffraction spots were obtained for CuO(P) and

CuO(H) nanoparticles which reveal the polycrystalline nature of the nanoparticles [39, 40]; however, from the SAED pattern of CuO(H) nanoparticles, it was exposed that it possesses the highest crystallinity and phase purity among the various nanoparticles prepared, and displaying single-crystalline nature [41]. The SAED pattern and the particle distribution graph for CuO(M), CuO(H) and CuO(P) nanoparticles are given in Fig. 4a–c.

### Raman analysis

The Raman spectra of three CuO nanoparticle samples, i.e. CuO(M), CuO(P) and CuO(H) were recorded and then given in Fig. 5. CuO has two molecules per unit primitive cell with space group symmetry  $C_{2h}^6$ . The equation associated with the lattice vibrations of a primitive cell is given as follows [42]:

$$\Gamma_{RA} = 4A_u + 5B_u + A_g + 2B_g. \quad (4)$$

There are 12 vibration modes predicted by group theory with only three active Raman modes, i.e.  $(A_g + 2B_g)$  and other are infra-red and acoustic modes given as  $(3A_u + 2B_u)$  and  $(A_u + 2B_u)$  [43]. The Raman spectra show  $A_g + 2B_g$  Raman active modes of CuO nanoparticles where  $A_g$  mode corresponds to phase rotations whereas first  $B_g$  mode is due to the bending of CuO, while second  $B_g$  mode is associated with symmetrical stretching of oxygen [44]. Raman peaks of CuO(P) nanoparticles are stronger and sharp in comparison to CuO(M) and CuO(H) nanoparticles which are due to grain size effect. The broadening and peak shift towards lower wavenumber are a result of grain size dependence of the Fourier coefficient of the phonon confinement function that is given by the equation [45].

$$|C(k)|^2 = e^{-\frac{k^2 d^2}{16\pi^2}}, \quad (5)$$

where  $C(k)$  is the Fourier coefficient of the phonon confinement function and  $d$  is the average crystallite size of the nanoparticles. It affects the frequency-dependent intensity of the Raman peak  $I(\omega)$  represented by the equation [45]:

$$I(\omega) = \int \frac{|C(0, k)|^2}{[\omega - \omega(k)]^2 + (I''/2)^2} d^3k, \quad (6)$$

where the three Raman modes arise due to the oxygen atoms vibration and spectra are independent of oxygen deficiency and significantly depend on the grain size [46, 47]. From the Raman spectra obtained, it was found that the CuO(M) nanoparticles yield peaks at 269  $\text{cm}^{-1}$  corresponding to the  $A_g$  and the 317  $\text{cm}^{-1}$  and 600  $\text{cm}^{-1}$  corresponding to the  $B_g$  (Fig. 5). However, upon observation of the Raman spectra of the samples CuO(P) and CuO(H), it can be observed there is a shift towards longer wave numbers indicating an increase in the grain size as confirmed by the TEM images [48]. Moreover, in the Raman spectra

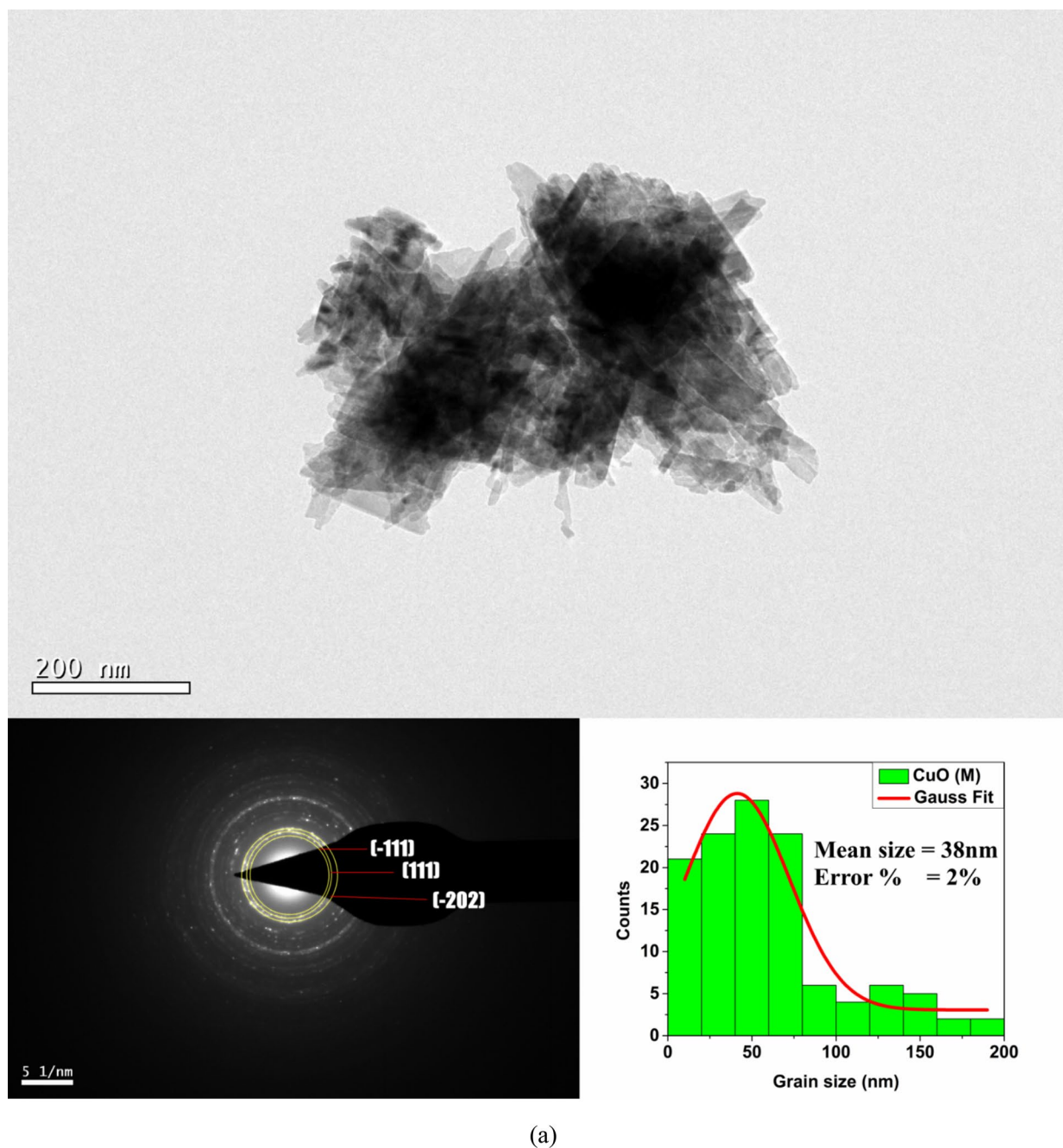


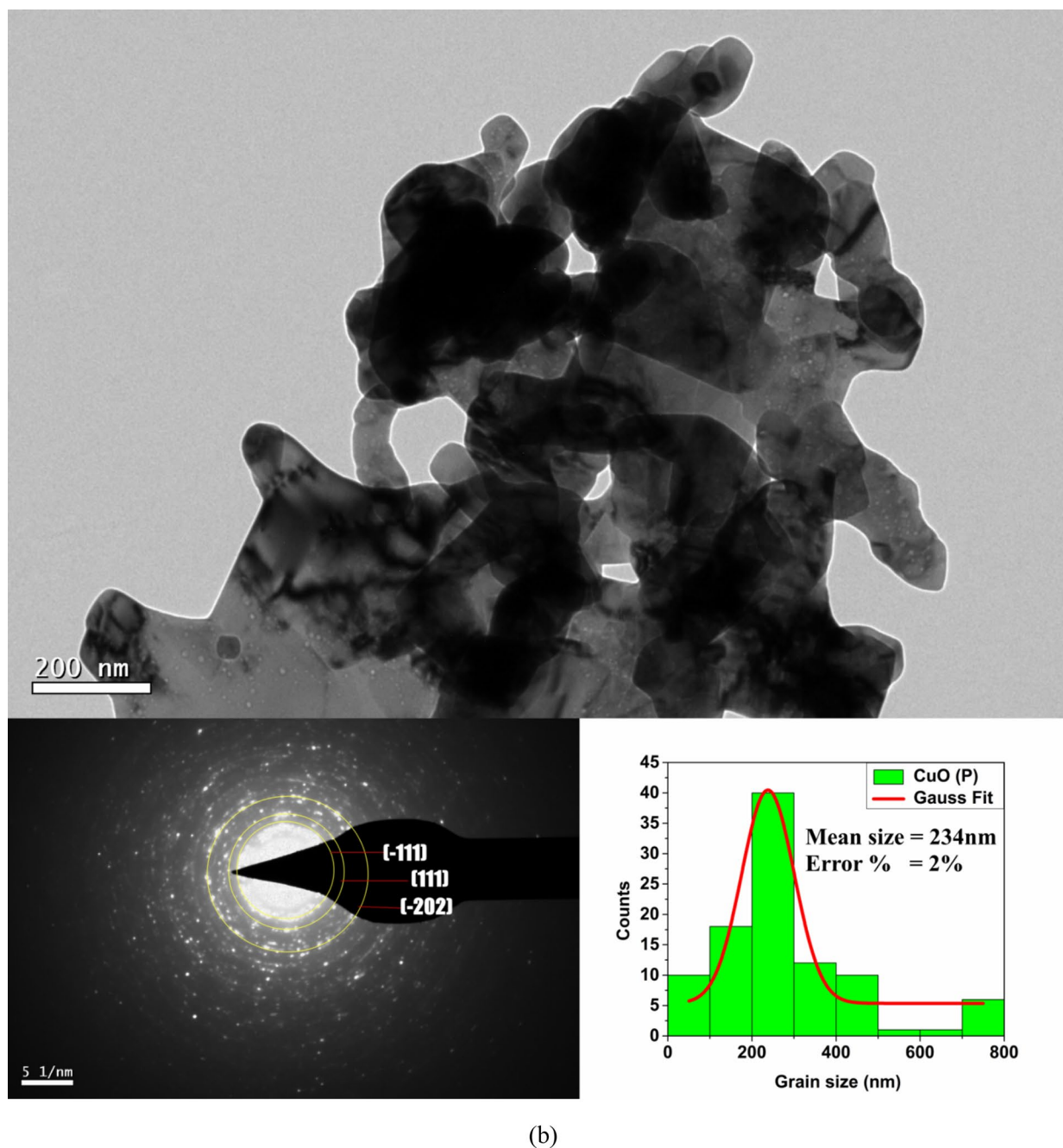
**Figure 4:** (a) TEM, SAED and images CuO (M) nanoparticles; (a) TEM, SAED and images CuO (P) nanoparticles; (a) TEM, SAED and images CuO (H) nanoparticles.

of the CuO(P) nanoparticle, sharper peaks have been obtained, which indicate possessing maximum percentage of oxygen vacancies as verified from XPS study.

### FTIR analysis

The presence of a broadband in the region  $3440\text{ cm}^{-1}$  to  $3450\text{ cm}^{-1}$  and  $1632\text{ cm}^{-1}$  to  $1634\text{ cm}^{-1}$  in all the synthesized samples is due to O–H stretching vibrations which are present

on the surface of CuO nanoparticles [49]. The presence of three peaks in the range of  $605\text{ cm}^{-1}$  to  $435\text{ cm}^{-1}$  can be ascribed to CuO bond stretching vibrations confirming the monoclinic cupric oxide formation in all the samples [50, 51]. The band at  $1384\text{ cm}^{-1}$  can be ascribed to C=O bond in all the prepared samples [49]. Hence, FTIR confirmed the purity of CuO nanoparticles prepared by different methods. Figure 6 shows the FTIR spectra of CuO(M), CuO(P) and CuO(H) nanoparticles.



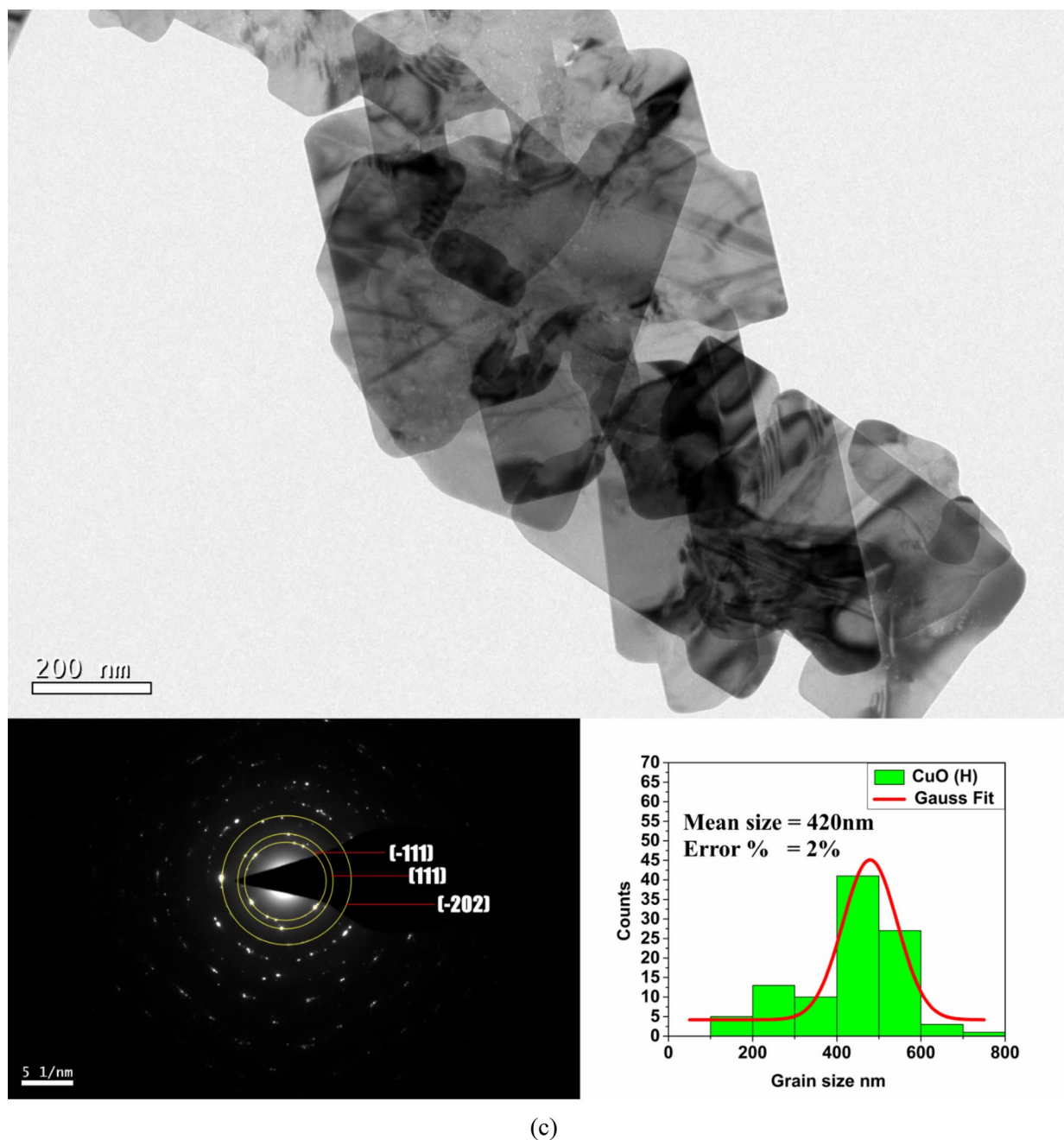
(b)

Figure 4: (continued)

**Antibacterial activity**

The alterations in the morphology and size of the CuO nanoparticles obtained by employing the various synthetic protocols were confirmed. A study of its effect on the antimicrobial efficiency of synthesized CuO NPs was evaluated against both Gram-negative, i.e. *Pseudomonas aeruginosa* MTCC 2453, *Klebsiella pneumonia* MTCC-39 and *Salmonella typhi* MTCC 734 and Gram-positive bacteria, i.e. *Staphylococcus aureus* MTCC 96, and this study was extended to the drug-resistant

strain MRSA, methicillin-resistant *Staphylococcus aureus* standard strain-CA 05 SCC mec Type IV as well. From the results obtained, it was observed that the antibacterial activity of the CuO nanoparticles was moderate against the Gram-negative bacteria, while it was found to be mild against the Gram-positive bacteria selected for the study. The inhibition zones (in mm) of varying sizes were obtained, as mentioned in Table 3 against *Pseudomonas aeruginosa*, *Klebsiella pneumoniae*, *Salmonella*



**Figure 4:** (continued)

*typhi* *Staphylococcus aureus* and MRSA and are illustrated graphically in Fig. 7a.

Interestingly, the CuO(M) nanoparticles displayed the best antimicrobial activity when compared to other nanoparticles, i.e. CuO(P) and CuO(H), which is in line with the study reported by Wu et al., in favour of Cu ions being involved in the antibacterial activity [52]; however, when compared with positive control i.e. ampicillin, the CuO nanoparticles tested display mild antimicrobial efficiency. In CuO(M) nanoparticles, maximum inhibition

zone was found against *K. pneumoniae* and minimum inhibition zone was found against *S. typhi*, both being Gram -ve bacterial strains. In case of the *S. aureus*, a Gram +ve bacterial strain, the zone of inhibition obtained was 18 mm which was lower than the 25 mm zone of inhibition obtained from the use of the positive control, i.e. ampicillin; moreover, a similar zone of inhibition was obtained when the drug-resistant strain, i.e. methicillin-resistant *S. aureus*, was tested employing CuO(M) nanoparticles, while the zone of inhibition for the control against



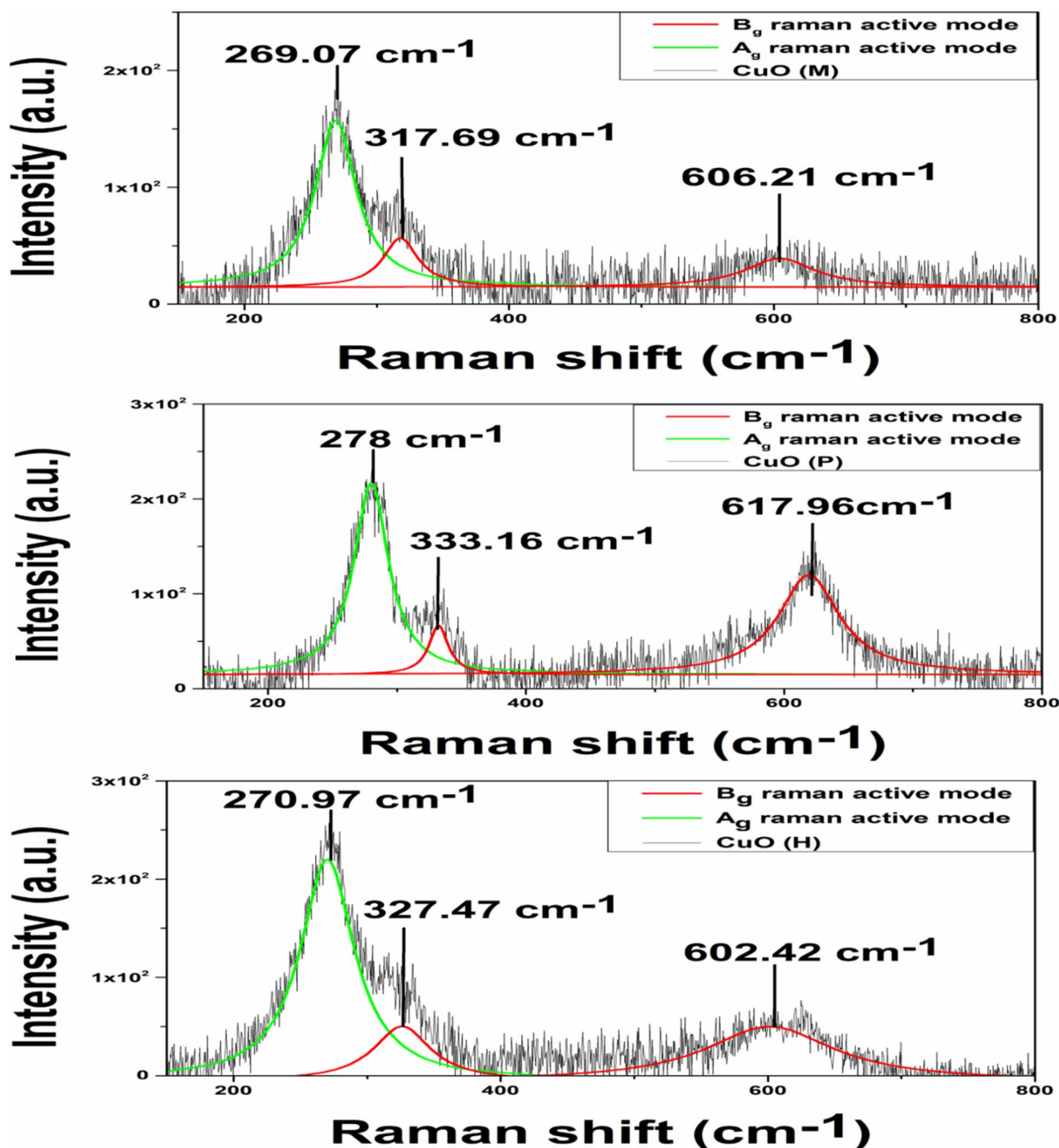


Figure 5: Raman spectra of CuO nanoparticles.

the resistant strain decreases, which indicates that the CuO(M) nanoparticles display equivalent efficiency against the regular stain as well as the drug-resistant strain. In the case of CuO(H) nanoparticles, maximum inhibition zone was found against *K. pneumoniae*, and minimum inhibition zone was found against *S. Typhi*. In the case of CuO(P) nanoparticles, maximum inhibition zone was found against *S. aureus* and minimum inhibition zone was found against *K. pneumoniae* and *S. Typhi*. In summary, the

results from the study indicate that CuO(M) nanoparticles are best among the nanoparticles prepared and the efficiency was found to be almost equivalent with that of antibiotic, which is according to Raghupathi et al., wherein it is reported that there exists an inverse relationship between antibacterial activity and nanoparticles size [53].

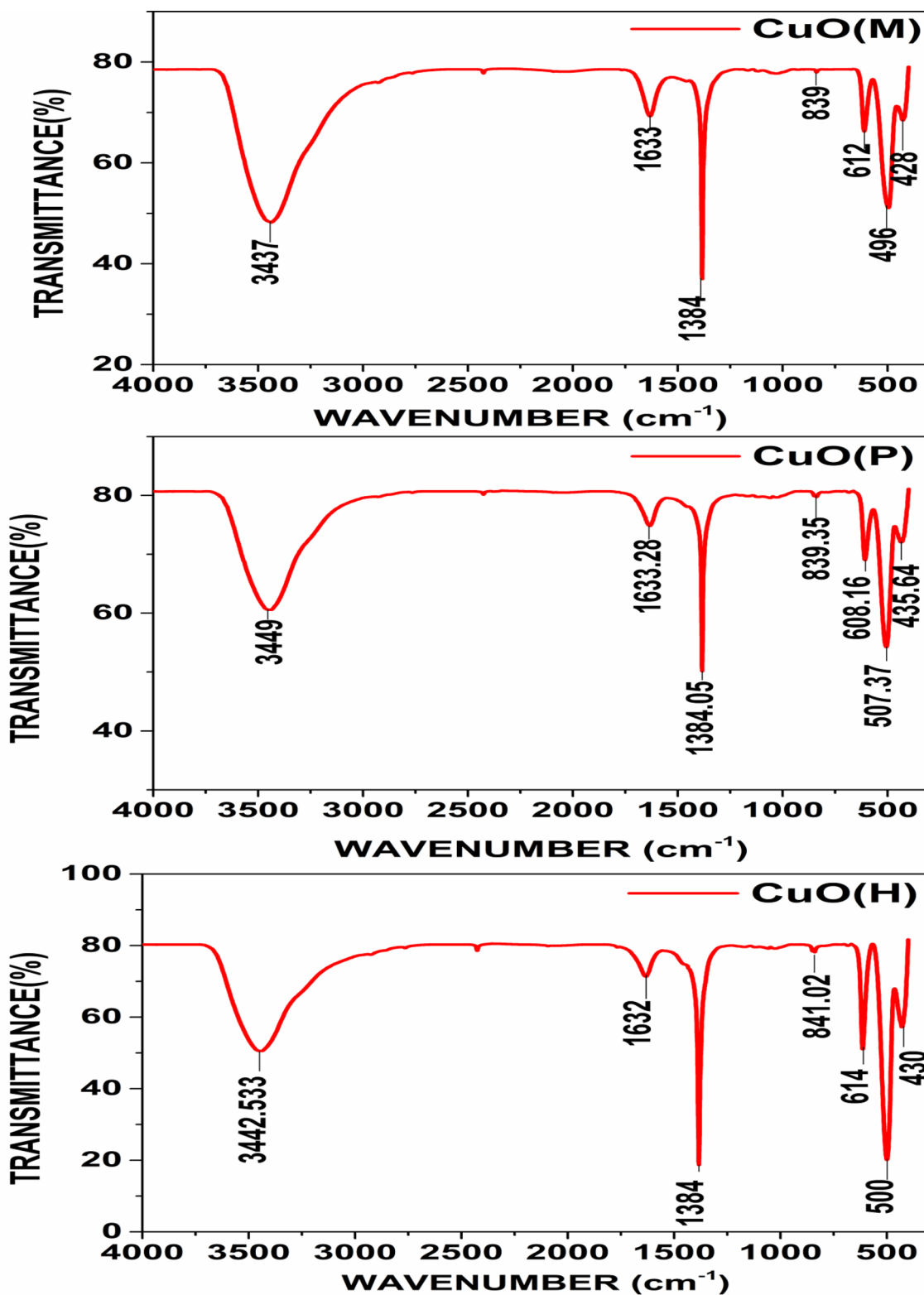
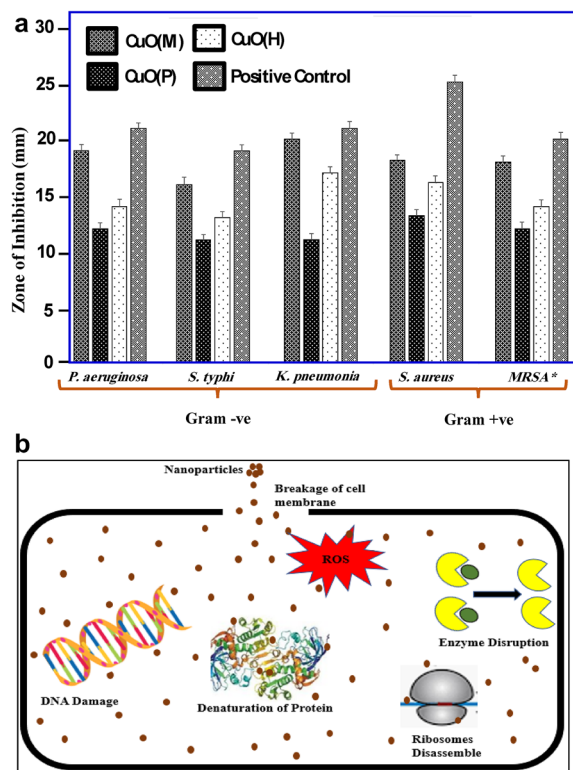


Figure 6: FTIR spectra of CuO nanoparticles.

**TABLE 3:** Inhibition zones obtained by employing CuO NPs against bacterial strains.

Bacterial strain	CuO(M)	CuO(P)	CuO(H)	Control		
				+ ve	- ve	
Gram - ve bacterial strains	<i>P. aeruginosa</i>	19 ± 0.553	12 ± 0.557	14 ± 0.638	21 ± 0.458	-
	<i>K. pneumoniae</i>	20 ± 0.559	11 ± 0.548	17 ± 0.572	21 ± 0.608	-
	<i>S. typhi</i>	16 ± 0.621	11 ± 0.528	13 ± 0.539	19 ± 0.561	-
Gram + ve bacterial strains	<i>S. aureus</i>	18 ± 0.448	13 ± 0.532	16 ± 0.583	25 ± 0.565	-
	Methicillin-resistant <i>S. aureus</i> (MRSA)	18 ± 0.53	12 ± 0.573	14 ± 0.562	20 ± 0.656	-



**Figure 7:** (a) Graphical representation of inhibition zones obtained by employing CuO NPs against bacterial strains; \*Methicillin-resistant *S. aureus* and (b) diagrammatic representation of antibacterial mechanism.

**Antibacterial mechanism**

Copper, a redox-active transition metal could labialize between two redox states oxidized cupric and reduced cuprous species [54]. According to various researchers, the antibacterial activity of metal oxide nanoparticles induces cell death by DNA damage, apoptosis alterations, cell cycle arrest followed by the release of metal ions into the bacterial cell [55, 56]. Metal oxide nanoparticles damage the cell membrane and DNA of microbes via diffusion. This damage includes the NP’s physical attachment to the DNA. A reason for antibacterial activity is also the generation of reactive oxygen species (ROS) by the nanoparticles attached to the bacterial cells, which in turn provoked an enhancement of the intracellular oxidative stress. The amount of ROS produced

by nanoparticles correlates with particle shape, size, chemistry and surface area. The main factors responsible for the production of ROS by nanoparticles include interaction with the mitochondria, interaction with NADPH oxidase and factors related to the physicochemical properties [57]. Different researchers suggested that Cu ions originating from the nanoparticles that interact with biomolecules containing sulfur and phosphorus such as protein and DNA to distort their structures and thus interfere with biochemical processes [58, 59]. The diagrammatically antibacterial mechanism of synthesized nanoparticles is shown in Fig. 7b.

**Conclusion**

The copper oxide nanoparticles were successfully synthesized using different synthesis routes such as microwave irradiation CuO(M), co-precipitation CuO(P), hydrothermal CuO(H) having monoclinic structure without any additional impurities and average crystallite size of 15.98 nm CuO(M), 23.02 nm CuO(P) and 21.88 nm CuO(H), respectively. Lower Chi<sup>2</sup> value approaching 1 of Rietveld refinement confirmed the crystal purity of the samples. XPS analysis revealed that CuO(P) nanoparticles did not contain chemisorbed oxygen and its presence influenced the antimicrobial property dependence of the nanoparticles. However, the microwave irradiation method synthesized nanoparticles with minimum crystallite size. The nanostructured phase formation was confirmed using Raman spectroscopy with the presence of all characteristic active Raman modes and lower particle size of the nanoparticles. The FTIR spectra confirmed the purity of CuO samples with no impurity phases. Further, as-synthesized nanoparticles were checked for their antibacterial properties. In CuO(M) and CuO(H) nanoparticles, maximum inhibition zone was found against *K. pneumoniae* whereas, in CuO(P) nanoparticles, maximum inhibition zone was found against *Staphylococcus aureus*. The antibacterial results revealed that CuO(M) nanoparticles had wide spectra of activity against Gram-positive bacteria and Gram-negative bacteria as compared to CuO(H) and CuO(P) nanoparticles. Hence, all the characteristic results of the CuO nanoparticles synthesized

using different techniques are in good agreement with each other and reveal that the antimicrobial property of CuO nanoparticles is size-dependent property.

## Materials and method

### Materials

All the chemicals used were of analytical grade (AR) and used without any further purification. Copper nitrate  $\text{Cu}(\text{NO}_3)_2$  (Merck), sodium hydroxide (NaOH) (Merck), ethylene glycol (Scientific Fisher) and triple distilled water were used for the synthesis of copper oxide nanoparticles.

### Method

Synthesis of CuO nanoparticles was performed through three different methods, viz. microwave irradiation CuO(M), co-precipitation CuO(P) and hydrothermal CuO(H). In brief 1 M, copper nitrate solution is taken and 10 M NaOH solution is added to it. In the case of microwave irradiation and hydrothermal protocol, this addition is carried out until a pH 9 is obtained, while in the co-precipitation method, the addition is continued until pH 11 is attained. For the microwave-mediated synthesis, the solution is placed in a microwave oven for 20 min at 40% power, while it is placed in a Teflon-lined autoclave for the hydrothermal synthesis at 120 °C for 24 h. In the case of the co-precipitation, the methodology the solution is stirred at 80 °C for 2 h. The dark brownish precipitate is obtained from the above three procedures which are centrifuged, washed several times. The solid obtained using the microwave-mediated synthesis and hydrothermal protocol is dried at 80 °C, unlike the co-precipitation method wherein the sample is calcined at 400 °C for 3 h in a muffle furnace. The experimental procedure is presented in the flowchart as shown in Fig. S7.

### Antibacterial activity of CuO nanoparticles

The nanoparticles were tested by the agar well diffusion method [60]. For antibacterial studies, the microbial strains *S. Typhi* (MTCC 734), *P. aeruginosa* (MTCC 2453) and *K. pneumonia* (MTCC-39), *S. aureus* (MTCC 96), and MRSA (methicillin-resistant *Staphylococcus aureus* standard strain-CA 05 SCCmec Type IV) were provided by parasitology laboratory of Shoolini University of Biotechnology and Management Sciences, Solan, India. In this study, nutrient agar was used as selective media whereas ampicillin was used as a positive control and triple distilled water was used as a negative control. The microbes were cultured in nutrient broth and incubated at a temperature of 37 °C for 12 to 18 h.

A solution of broth microbial culture was prepared, which was then blown out on nutrient agar plates. The plates were left undisturbed for 10–15 min to enhance culture absorption. With a sterile puncher, the wells (10 mm size) were pierced into the agar. A solution of CuO nanoparticles and solution of positive control (ampicillin) and negative control (triple distilled water) were taken and then shifted to the wells kept in all plates. The incubation was carried out at a temperature of 37 °C for 18 to 24 h. The size of the inhibition zone was measured and the analysis was repeated for three replicates.

### Characterization

The phase formation and purity of the compounds were verified with the help of X-ray diffraction (XRD) Rigaku Miniflex-600, Japan, with CuK $\alpha$  radiation ( $\lambda = 1.5405 \text{ \AA}$ ) between 20 and 60 °C at a scanning rate of 2°/min at room temperature.

### Acknowledgments

Author K M Bato is thankful to the Deanship of Scientific Research at King Saud University for financial support through the project Code (RG-1437-030).

### Data availability

All data generated or analysed during this study are included in this published article and in supplementary file.

### Declarations

**Conflict of interest** Authors declare that they have no conflict of interest among them.

### Supplementary Information

The online version contains supplementary material available at <https://doi.org/10.1557/s43578-021-00193-7>.

### References

1. Y. Liu, Q. Huang, G. Jiang, D. Liu, W. Yu, Cu 2 O nanoparticles supported on carbon nanofibers as a cost-effective and efficient catalyst for RhB and phenol degradation. *J. Mater. Res.* **32**, 3605–3615 (2017)
2. K. Vishveshvar, M.A. Krishnan, K. Haribabu, S. Vishnuprasad, Green synthesis of copper oxide nanoparticles using ixiro coc-cinea plant leaves and its characterization. *BioNanoScience* **8**, 554–558 (2018)
3. M. Khan, M.R. Shaik, S.F. Adil, M. Kuniyil, M. Ashraf, H. Fre-richs et al., Facile synthesis of Pd@ graphene nanocomposites

- with enhanced catalytic activity towards Suzuki coupling reaction. *Sci. Rep.* **10**, 1–14 (2020)
4. K. Gherab, Y. Al-Douri, U. Hashim, M. Ameri, A. Bouhemadou, K.M. Batoou et al., Fabrication and characterizations of Al nanoparticles doped ZnO nanostructures-based integrated electrochemical biosensor. *J. Market. Res.* **9**, 857–867 (2020)
  5. S.M. Boddapati, J.M.R. Saketi, B.R. Mutchu, H.B. Bollikolla, S.F. Adil, M. Khan, Copper promoted desulfurization and CN cross coupling reactions: Simple approach to the synthesis of substituted 2-aminobenzoxazoles and 2, 5-disubstituted tetrazole amines. *Arab. J. Chem.* **13**, 4477–4494 (2020)
  6. S.F. Adil, M.E. Assal, M.R. Shaik, M. Kuniyil, N.M. AlOtaibi, M. Khan et al., A facile synthesis of ZrO<sub>x</sub>-MnCO<sub>3</sub>/graphene oxide (GRO) nanocomposites for the oxidation of alcohols using molecular oxygen under base free conditions. *Catalysts* **9**, 759 (2019)
  7. S. Kumar, R. Rani, N. Dilbaghi, K. Tankeshwar, K.-H. Kim, Carbon nanotubes: a novel material for multifaceted applications in human healthcare. *Chem. Soc. Rev.* **46**, 158–196 (2017)
  8. S. Kumar, W. Ahlawat, G. Bhanjana, S. Heydarifard, M.M. Nazhad, N. Dilbaghi, Nanotechnology-based water treatment strategies. *J. Nanosci. Nanotechnol.* **14**, 1838–1858 (2014)
  9. N.D. Mu'azu, N. Jarrah, M. Zubair, M.S. Manzar, T.S. Kazeem, A. Qureshi et al., Mechanistic aspects of magnetic MgAlNi barium-ferrite nanocomposites enhanced adsorptive removal of an anionic dye from aqueous phase. *J. Saudi Chem. Soc.* **24**, 715–732 (2020)
  10. S. Saif, A. Tahir, T. Asim, Y. Chen, S.F. Adil, Polymeric nanocomposites of iron-oxide nanoparticles (IONPs) synthesized using terminalia chebula leaf extract for enhanced adsorption of arsenic (V) from water. *Colloids Interfaces* **3**, 17 (2019)
  11. M. Signoretto, F. Menegazzo, A. Di Michele, E. Fioriniello, Effects of support and synthetic procedure for sol-immobilized Au nanoparticles. *Catalysts* **6**, 87 (2016)
  12. M.S. Bakshi, How surfactants control crystal growth of nanomaterials. *Cryst. Growth Des.* **16**, 1104–1133 (2016)
  13. Y. Li, C. Li, B. Wang, W. Li, P. Che, A comparative study on the thermoelectric properties of CoSb<sub>3</sub> prepared by hydrothermal and solvothermal route. *J. Alloy. Compd.* **772**, 770–774 (2019)
  14. J.Y. Cheon, S.J. Kim, Y.H. Rhee, O.H. Kwon, W.H. Park, Shape-dependent antimicrobial activities of silver nanoparticles. *Int. J. Nanomed.* **14**, 2773 (2019)
  15. J.J. Lv, M.Y. Li, and Q.X. Zeng, Preparation and characterization of copper oxide and copper nanoparticles. in *Advanced Materials Research*, 2011, pp. 715–721
  16. N. Dhineshbabu, V. Rajendran, N. Nithyavathy, R. Vetumperumal, Study of structural and optical properties of cupric oxide nanoparticles. *Appl. Nanosci.* **6**, 933–939 (2016)
  17. J.K. Sharma, M.S. Akhtar, S. Ameen, P. Srivastava, G. Singh, Green synthesis of CuO nanoparticles with leaf extract of *Calotropis gigantea* and its dye-sensitized solar cells applications. *J. Alloy. Compd.* **632**, 321–325 (2015)
  18. O. Waser, M. Hess, A. Grntner, P. Novßk, S.E. Pratsinis, Size controlled CuO nanoparticles for Li-ion batteries. *J. Power Sources* **241**, 415–422 (2013)
  19. F. Wang, H. Li, Z. Yuan, Y. Sun, F. Chang, H. Deng et al., A highly sensitive gas sensor based on CuO nanoparticles synthesized via a sol-gel method. *RSC Adv.* **6**, 79343–79349 (2016)
  20. M. Shahmiri, N.A. Ibrahim, F. Shayesteh, N. Asim, N. Motallebi, Preparation of PVP-coated copper oxide nanosheets as antibacterial and antifungal agents. *J. Mater. Res.* **28**, 3109 (2013)
  21. P. Sutradhar, M. Saha, D. Maiti, Microwave synthesis of copper oxide nanoparticles using tea leaf and coffee powder extracts and its antibacterial activity. *J. Nanostruct. Chem.* **4**, 86 (2014)
  22. C. Boruban, E.N. Esenturk, Synthesis of CuO nanostructures on zeolite-Y and investigation of their CO<sub>2</sub> adsorption properties. *J. Mater. Res.* **32**, 3669 (2017)
  23. G. Mustafa, H. Tahir, M. Sultan, N. Akhtar, Synthesis and characterization of cupric oxide (CuO) nanoparticles and their application for the removal of dyes. *Afr. J. Biotechnol.* **12**, 6650–6660 (2013)
  24. R. Sankar, R. Maheswari, S. Karthik, K.S. Shivashangari, V. Ravikumar, Anticancer activity of *Ficus religiosa* engineered copper oxide nanoparticles. *Mater. Sci. Eng. C* **44**, 234–239 (2014)
  25. A. Hussain, M.F. AlAjmi, M.T. Rehman, S. Amir, F.M. Husain, A. Alsalmeh et al., Copper (II) complexes as potential anticancer and nonsteroidal anti-inflammatory agents: in vitro and in vivo studies. *Sci. Rep.* **9**, 1–17 (2019)
  26. C.L. Carnes, K.J. Klabunde, The catalytic methanol synthesis over nanoparticle metal oxide catalysts. *J. Mol. Catal. A* **194**, 227–236 (2003)
  27. L. Sun, Z. Zhang, Z. Wang, Z. Wu, H. Dang, Synthesis and characterization of CuO nanoparticles from liquid ammonia. *Mater. Res. Bull.* **40**, 1024–1027 (2005)
  28. P. Saravanan, S. Alam, G. Mathur, A liquid-liquid interface technique to form films of CuO nanowhiskers. *Thin Solid Films* **491**, 168–172 (2005)
  29. T. Ahmad, R. Chopra, K. Ramanujachary, S. Lofland, A. Ganguli, Canted antiferromagnetism in copper oxide nanoparticles synthesized by the reverse-micellar route. *Solid State Sci.* **7**, 891–895 (2005)
  30. V.V.T. Padil, M. Černík, Green synthesis of copper oxide nanoparticles using gum karaya as a biotemplate and their antibacterial application. *Int. J. Nanomed.* **8**, 889 (2013)
  31. B.D. Cullity, *Elements of X-Ray Diffraction* (Addison-Wesley Publishing, Boston, 1956).
  32. E.E. Kaya, S. Gürmen, A straightforward approach for the synthesis of nanostructured Y<sub>2</sub>O<sub>3</sub> particles: synthesis, morphology,

- microstructure and crystal imperfection. *Phys. E*. **115**, 113668 (2020)
33. V. Mote, Y. Purushotham, B. Dole, Williamson-Hall analysis in estimation of lattice strain in nanometer-sized ZnO particles. *J. Theoret. Appl. Phys.* **6**, 6 (2012)
  34. G. Rajender, P. Giri, Strain induced phase formation, microstructural evolution and bandgap narrowing in strained TiO<sub>2</sub> nanocrystals grown by ball milling. *J. Alloy. Compd.* **676**, 591–600 (2016)
  35. A. Chauhan, R. Verma, S. Kumari, A. Sharma, P. Shandilya, X. Li et al., Photocatalytic dye degradation and antimicrobial activities of pure and Ag-doped ZnO using *Cannabis sativa* leaf extract. *Sci. Rep.* **10**, 1–16 (2020)
  36. P. Bindu, S. Thomas, Estimation of lattice strain in ZnO nanoparticles: X-ray peak profile analysis. *J. Theoret. Appl. Phys.* **8**, 123–134 (2014)
  37. Y. Asakuma, M. Miura, Effect of microwave radiation on diffusion behavior of anti-solvent during crystallization. *J. Cryst. Growth* **402**, 32–36 (2014)
  38. Y. Wang, Y. Lü, W. Zhan, Z. Xie, Q. Kuang, L. Zheng, Synthesis of porous Cu<sub>2</sub>O/CuO cages using Cu-based metal–organic frameworks as templates and their gas-sensing properties. *J. Mater. Chem. A* **3**, 12796–12803 (2015)
  39. R. Mariammal, K. Ramachandran, B. Renganathan, D. Sastikumar, On the enhancement of ethanol sensing by CuO modified SnO<sub>2</sub> nanoparticles using fiber-optic sensor. *Sens. Actuators B* **169**, 199–207 (2012)
  40. D.D.M. Prabakaran, K. Sadaiyandi, M. Mahendran, S. Sagadevan, Precipitation method and characterization of cobalt oxide nanoparticles. *Appl. Phys. A* **123**, 264 (2017)
  41. H. Siddiqui, M. Qureshi, F.Z. Haque, Effect of copper precursor salts: facile and sustainable synthesis of controlled shaped copper oxide nanoparticles. *Optik* **127**, 4726–4730 (2016)
  42. M. Dar, Q. Ahsanulhaq, Y. Kim, J. Sohn, W. Kim, H. Shin, Versatile synthesis of rectangular shaped nanoball-like CuO nanostructures by hydrothermal method; structural properties and growth mechanism. *Appl. Surf. Sci.* **255**, 6279–6284 (2009)
  43. J.D. Rodney, S. Deepapriya, P.A. Vinosha, S. Krishnan, S.J. Priscilla, R. Daniel et al., Photo-Fenton degradation of nano-structured La doped CuO nanoparticles synthesized by combustion technique. *Optik* **161**, 204–216 (2018)
  44. H. Siddiqui, M.R. Parra, F.Z. Haque, Optimization of process parameters and its effect on structure and morphology of CuO nanoparticle synthesized via the sol–gel technique. *J. Sol-Gel. Sci. Technol.* **87**, 125–135 (2018)
  45. A. Bhaumik, A.M. Shearin, R. Patel, K. Ghosh, Significant enhancement of optical absorption through nano-structuring of copper based oxide semiconductors: possible future materials for solar energy applications. *Phys. Chem. Chem. Phys.* **16**, 11054–11066 (2014)
  46. J. Irwin, T. Wei, Raman scattering investigation of Cu<sub>18</sub>O. *J. Phys.* **3**, 299 (1991)
  47. J. Xu, W. Ji, Z. Shen, W. Li, S. Tang, X. Ye et al., Raman spectra of CuO nanocrystals. *J. Raman Spectrosc.* **30**, 413–415 (1999)
  48. M. Rashad, M. Rüsing, G. Berth, K. Lischka, and A. Pawlis, CuO and Co<sub>3</sub>O<sub>4</sub> nanoparticles: synthesis, characterizations, and Raman spectroscopy. *J. Nanomater.* **2013** (2013)
  49. Z.N. Kayani, M. Umer, S. Riaz, S. Naseem, Characterization of copper oxide nanoparticles fabricated by the sol–gel method. *J. Electron. Mater.* **44**, 3704–3709 (2015)
  50. R. Jana, A. Dey, M. Das, J. Datta, P. Das, P.P. Ray, Improving performance of device made up of CuO nanoparticles synthesized by hydrothermal over the reflux method. *Appl. Surf. Sci.* **452**, 155–164 (2018)
  51. A. Bhattacharjee, M. Ahmaruzzaman, Microwave assisted facile and green route for synthesis of CuO nanoleaves and their efficacy as a catalyst for reduction and degradation of hazardous organic compounds. *J. Photochem. Photobiol. A* **353**, 215–228 (2018)
  52. X. Wu, L. Ye, K. Liu, W. Wang, J. Wei, F. Chen et al., Antibacterial properties of mesoporous copper-doped silica xerogels. *Biomed. Mater.* **4**, 045008 (2009)
  53. K.R. Raghupathi, R.T. Koodali, A.C. Manna, Size-dependent bacterial growth inhibition and mechanism of antibacterial activity of zinc oxide nanoparticles. *Langmuir* **27**, 4020–4028 (2011)
  54. J.E. Weckx, H.M. Clijsters, Oxidative damage and defense mechanisms in primary leaves of *Phaseolus vulgaris* as a result of root assimilation of toxic amounts of copper. *Physiol. Plant.* **96**, 506–512 (1996)
  55. R. Brayner, R. Ferrari-Iliou, N. Brivois, S. Djediat, M.F. Benedetti, F. Fiévet, Toxicological impact studies based on *Escherichia coli* bacteria in ultrafine ZnO nanoparticles colloidal medium. *Nano Lett.* **6**, 866–870 (2006)
  56. Z. Huang, X. Zheng, D. Yan, G. Yin, X. Liao, Y. Kang et al., Toxicological effect of ZnO nanoparticles based on bacteria. *Langmuir* **24**, 4140–4144 (2008)
  57. A. Abdal Dayem, M.K. Hossain, S.B. Lee, K. Kim, S.K. Saha, G.-M. Yang et al., The role of reactive oxygen species (ROS) in the biological activities of metallic nanoparticles. *Int. J. Mol. Sci.* **18**, 120 (2017)
  58. M. Raffi, S. Mehrwan, T.M. Bhatti, J.I. Akhter, A. Hameed, W. Yawar et al., Investigations into the antibacterial behavior of copper nanoparticles against *Escherichia coli*. *Ann. Microbiol.* **60**, 75–80 (2010)
  59. J.P. Ruparelia, A.K. Chatterjee, S.P. Duttagupta, S. Mukherji, Strain specificity in antimicrobial activity of silver and copper nanoparticles. *Acta Biomater.* **4**, 707–716 (2008)
  60. R. Verma, A. Chauhan, M. Shandilya, X. Li, R. Kumar, S. Kulshrestha, Antimicrobial potential of Ag-doped ZnO nanostructure synthesized by the green method using *Moringa oleifera* extract. *J. Environ. Chem. Eng.* **8**, 103730 (2020)